



HAL
open science

Coherent Anti-Stokes Raman Scattering Microscopy: A Label-Free Method to Compare Spinal Cord Myelin in Different Species

Gaëtan Poulen, Yannick N Gerber, Jean-Christophe Perez, Khadidja Oubarrahou, Nicolas Lonjon, Florence Vachiere-Lahaye, Hassan Boukhaddaoui, Florence E. Perrin

► To cite this version:

Gaëtan Poulen, Yannick N Gerber, Jean-Christophe Perez, Khadidja Oubarrahou, Nicolas Lonjon, et al.. Coherent Anti-Stokes Raman Scattering Microscopy: A Label-Free Method to Compare Spinal Cord Myelin in Different Species. *Frontiers in Physics*, 2021, 9, 10.3389/fphy.2021.665650 . hal-03475946

HAL Id: hal-03475946

<https://hal.science/hal-03475946>

Submitted on 11 Dec 2021

HAL is a multi-disciplinary open access archive for the deposit and dissemination of scientific research documents, whether they are published or not. The documents may come from teaching and research institutions in France or abroad, or from public or private research centers.

L'archive ouverte pluridisciplinaire **HAL**, est destinée au dépôt et à la diffusion de documents scientifiques de niveau recherche, publiés ou non, émanant des établissements d'enseignement et de recherche français ou étrangers, des laboratoires publics ou privés.



Coherent Anti-Stokes Raman Scattering Microscopy: A Label-Free Method to Compare Spinal Cord Myelin in Different Species

Gaëtan Poulen¹, Yannick N Gerber², Jean-Christophe Perez², Khadidja Oubarrahou³, Nicolas Lonjon¹, Florence Vachieri-Lahaye⁴, Hassan Boukhaddaoui³ and Florence E. Perrin^{2,5*}

¹Department of Neurosurgery, MMDN, EPHE, INSERM, University de Montpellier, Montpellier, France, ²MMDN, University de Montpellier, EPHE, INSERM, Montpellier, France, ³Institute for Neurosciences of Montpellier, INSERM, Montpellier, France, ⁴Department of Coordination Hospitalière des Dons pour La Greffe, Montpellier, France, ⁵Institut Universitaire de France (IUF), Montpellier, France

OPEN ACCESS

Edited by:

Peng Gao,
Xidian University, China

Reviewed by:

Nirmal Mazumder,
Manipal Academy of Higher
Education, India
Sha AnXian,
Institute of Optics and Precision
Mechanics (CAS), China

*Correspondence:

Florence E. Perrin
florence.perrin@inserm.fr

Specialty section:

This article was submitted to
Optics and Photonics,
a section of the journal
Frontiers in Physics

Received: 08 February 2021

Accepted: 21 July 2021

Published: 30 September 2021

Citation:

Poulen G, Gerber YN, Perez J-C,
Oubarrahou K, Lonjon N,
Vachieri-Lahaye F, Boukhaddaoui H
and Perrin FE (2021) Coherent Anti-
Stokes Raman Scattering Microscopy:
A Label-Free Method to Compare
Spinal Cord Myelin in Different Species.
Front. Phys. 9:665650.
doi: 10.3389/fphy.2021.665650

Many histological techniques are used to identify and characterize myelin in the mammalian nervous system. Due to the high content of lipids in myelin sheaths, coherent anti-stokes Raman scattering (CARS) microscopy is a label-free method that allows identifying myelin within tissues. CARS excites the CH₂ vibrational mode at 2845 cm⁻¹ and CH₂ bonds are found in lipids. In this study, we have used CARS for a new biological application in the field of spinal cord analysis. We have indeed compared several parameters of spinal cord myelin sheath in three different species, *i.e.*, mouse, lemur, and human using a label-free method. In all species, we analyzed the dorsal and the lateral *funiculi* of the adult thoracic spinal cord. We identified g-ratio differences between species. Indeed, in both *funiculi*, g-ratio was higher in mice than in the two primate species, and the myelin g-ratio in lemurs was higher than in humans. We also detected a difference in g-ratio between the dorsal and the lateral *funiculi* only in humans. Furthermore, species differences between axon and fiber diameters as well as myelin thickness were observed. These data may reflect species specificities of conduction velocity of myelin fibers. A comparison of data obtained by CARS imaging and fluoromyelin staining, a method that, similar to CARS, does not require resin embedding and dehydration, displays similar results. CARS is, therefore, a label-free alternative to other microscopy techniques to characterize myelin in healthy and neurological disorders affecting the spinal cord.

Keywords: myelinated fibers, g-ratio, CARS, spinal cord, human, lemur, mice

INTRODUCTION

Myelin is a lipid-rich protective cover formed by oligodendrocytes that surround and protect axons. Lipids account for about 70% of the myelin and myelin sheaths are characterized by a high lipid-to-protein ratio. Furthermore, myelin displays different lipid compositions when compared to typical plasma membranes [1,2]. Myelin sheaths permit to increase the propagation speed of action potentials along axons [3,4]. Moreover, myelin is a dynamic structure spatially organized in heterogeneous functional domains that provide metabolic support to neurons [5].

Loss and alteration of myelin that results in the reduction of nerve conduction velocity and in the altered transfer of energy metabolites to neurons are reported in various diseases [6,7]. Damage to myelin sheaths

in humans is observed in severe neurological conditions such as multiple sclerosis, idiopathic inflammatory demyelinating diseases, acute disseminated encephalomyelitis, and neuromyelitis *optica* [4,8].

To identify myelin on tissues, on the one hand, classical staining based on the specific lipid composition of myelin, such as Luxol fast blue [9], Sudan Black B [10], Baker's acid hematin method [11], and silver staining [12], had been originally developed. However, these stainings do not always reach a sufficient resolution and contrast to visualize individual fibers [13]. On the other hand, immunochemical methods permit to characterize myelin structure with single fiber resolution and a high reproducibility. Antimyelin protein antibodies most commonly used are myelin basic protein (MBP), proteolipid protein (PLP), myelin oligodendrocyte glycoprotein (MOG), myelin protein zero (MPZ), and myelin-associated glycoprotein [14]. As for all immunohistochemistry approaches, drawbacks are the potential lack of specificity and background noise. Moreover, they only permit a semiquantitative quantification.

Coherent anti-Stokes Raman scattering (CARS) microscopy is a nonlinear optical technique using the endogenous contrast provided by molecules present in the sample [15–17]. The major advantage of this technique is to be done directly on tissues without staining, dehydration, and embedding steps that are detrimental to myelin preservation [18]. Lipid-rich myelinated tissues, such as the spinal cord and brain, appeared to be good samples for CARS imaging [19]. CARS had been used to develop an automated method for the segmentation and morphometric analysis of nerve fibers of spinal cord tissue [20]. CARS had also been used to monitor live myelinated fibers [21], *in vivo* mouse brain [22], and to carry out a longitudinal *in vivo* follow-up of demyelination and remyelination in the injured rats' spinal cord [23]. CARS also permitted to characterize demyelination in mouse models of diseases such as amyotrophic lateral sclerosis [24], experimental autoimmune encephalomyelitis [25], and brain tissues of multiple sclerosis patients [26].

This is the first study using a label-free method to compare myelin sheaths of two separated spinal cord tracts in three different species, i.e., mice, lemurs, and humans. Direct comparison of myelin characteristics between species will not only provide basic data on their similarities but also open the way to compare myelin alterations in animal models and human diseases.

METHODS

Study approval: Experiments were approved by the Veterinary Services Department of Hérault, the regional ethic committee n°36 for animal experimentation, and the French Ministry of National Education, Higher Education and Research (authorizations; mice: n°34118 and non-human primates n° APAFIS#16177-2018071810113615v3). Experiments followed the European legislative, administrative, and statutory measures for animal experimentation (EU/Directive/2010/63) and the ARRIVE guidelines. Human samples collection was done under the approval of the “Agence de la Biomédecine” (PFS-ssNUM-BAUCHET).

Spinal Cord Samples

Animals were injected with a lethal dose of tribromoethanol (rodent; 500 mg/kg, Sigma Aldrich Darmstadt, Germany) or

ketamine (non-human primates; 150 mg/kg, Merial, Lyon, France). Animals were perfused intracardially with cold phosphate saline buffer (PBS, 0.1 M, pH 7.2) followed by cold 4% paraformaldehyde (PFA, pH7.2, Sigma Aldrich, Darmstadt, Germany) in 0.1 M PBS. Spinal cords were post-fixed for 2 h in 4% PFA and then incubated in 30% sucrose in 0.1 M PBS, frozen in OCT (Sakura, Alphen aan den Rijn, Netherlands) and stored at -20°C .

Mice: Three C57BL6/6J male mice of 3 months of age (Charles River, Wilmington, United States) were used. Non-human primates: three adult male lemurs (*Microcebus murinus*, 2 years old) were used. They were born and bred in the animal facility (the University of Montpellier, France (license approval 34-05-026-FS) and housed in cages equipped with wooden nests and an enriched environment. The temperature of the animal facility was constantly kept between 24–26°C with 55% of humidity. All *Microcebus murinus* were fed 3 times a week with fresh fruits and a mixture of cereal, milk, and eggs. Water was given *ad libitum*.

Human: Low thoracic (T11–T12) spinal cords were obtained from three brain-dead organ-donor patients (2 males 45 and 51 years and 1 female 68 years) under the approval of the French Institution for Organ Transplantation. One patient died from cardiac arrest and two from a ruptured aneurysm. Body temperature was lowered and blood circulation and ventilation were maintained until 4 h before spinal cord removal. This short-time interval permitted good preservation of the tissue, as already reported [27]. After organs removal for therapeutic purposes, T8–L5 vertebral bloc was isolated and spinal cord segments were removed and immediately fixed in 4% paraformaldehyde.

Luxol Fast Blue and Neutral Red Staining

14- μm -thick axial spinal cord cryosections (Microm HM550, ThermoFisher Scientific, Waltham, United States) were collected on Superfrost Plus® slides. Luxol fast blue staining was done as previously described [28,29]. Briefly, sections were placed 5 min in 95% ethanol and then incubated in 0.1% Luxol fast blue under mild shaking (12 h, room temperature). Slides were then rinsed for 1 min in milli-Q water, then placed for 1 min in lithium carbonate (0.05%), and finally washed in tap water (1 min). Subsequently, slides were incubated for 10 min in 0.5% neutral red solution, 5 min in 100% ethanol, and washed twice for 10 min in xylene. All slides were cover-slipped using Eukitt (Sigma Aldrich, Darmstadt, Germany).

Coherent Anti-Stokes Raman Scattering and Quantifications

We used LSM 7 MP optical parametric oscillator (OPO) multiphoton microscope (Zeiss, Oberkochen, Germany) with an upright Axio Examiner Z.1 optical microscope associated with a femtosecond Ti: sapphire laser (680–1,080 nm, 80 MHz, 140 fs, Chameleon Ultra II, Coherent, France) pumping a tunable OPOs (1,000–1,500 nm, 80 MHz, 200 fs, Chameleon Compact OPO, Coherent, France) to acquire CARS images. We imaged axial spinal cord sections (14 μm) in all species. A x20 water immersion lens (W Plan Apochromat DIC VIS-IR) with the following characteristics: 1024 x 1024 pixels frame size, scan speed of 6 (zoom x1.2) and 8 (mosaic, zoom x3, PixelDwell 3.15 and 1.27 $\mu\text{s}/\text{scan}$, respectively) and either a zoom x1.2 or x3 was

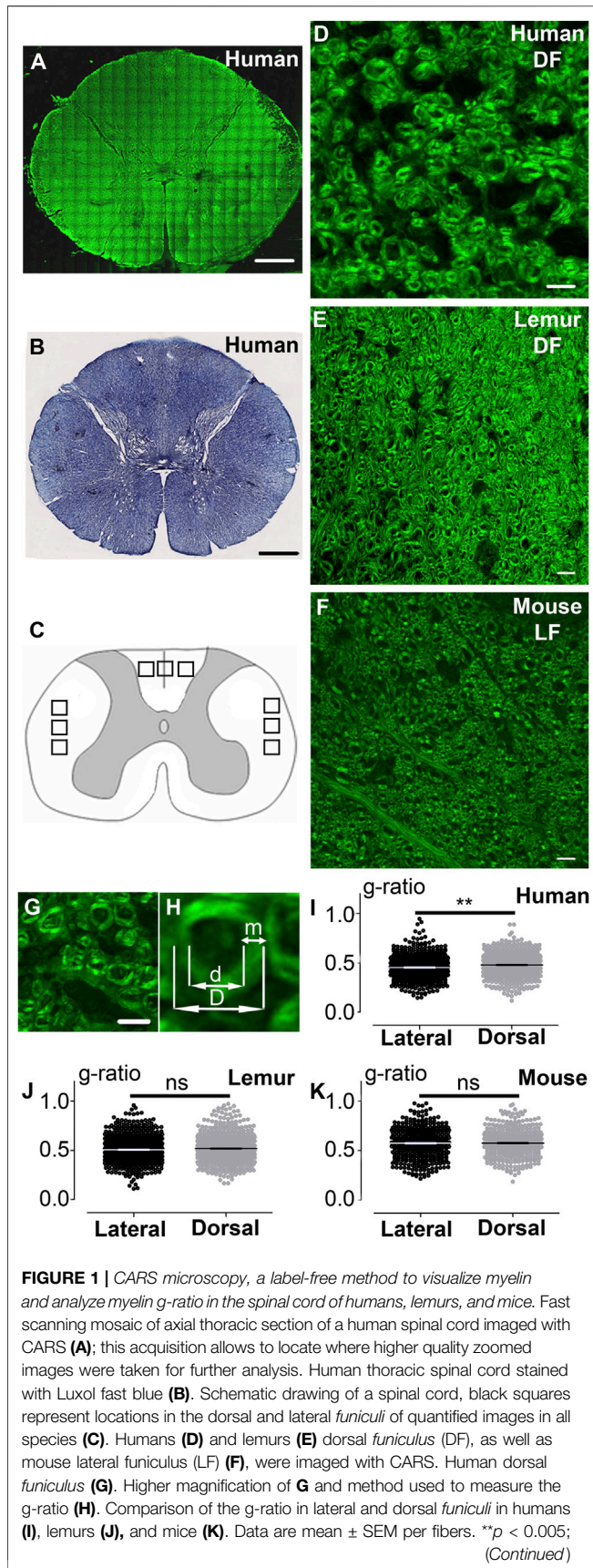


FIGURE 1 | paired *t*-test. The number of fibers analyzed: *n* is at least 432 and up to 681 per group; however, in a given species, the number of fibers in LF and DF is similar. In all graphs, quantification in the lateral funiculus is in black and the dorsal funiculus is in light grey. Scale bars: (A, B) 1 mm, (D–G) 10 μ m.

used. CARS excites the CH_2 vibrational mode at 2845 cm^{-1} and CH_2 bonds are found in lipids and thus in myelin sheath [30]. Excitation wavelengths are 836 and 1,097 nm (synchronized Ti-sapphire and OPO, respectively) and the signal is detected at 675 nm (filter from 660–685 nm).

The non-resonant background is reduced due to the use of femtosecond impulsive [31,32] and EPI-detection [33] [for review see [34]]. We collected CARS signaling in the near-infrared (670 nm) since this wavelength produces rather limited autofluorescence when using biological tissue. Moreover, and as previously reported, before getting a simultaneous scan of both lasers, we switch off sequentially one of the laser beams (either OPO or Ti : sapphire) to confirm a robust intensity decay when compared to the CARS signal [30].

Pictures are a stack of $3 \mu\text{m}$ (3 slices) and were taken in six locations within the lateral funiculus and three locations in the dorsal funiculus (Figure 1C). In each picture, a square of $100 \mu\text{m} \times 100 \mu\text{m}$ located in the center of the image was quantified. Imaris 9.6.0 software was used (Bitplane AG, Zurich, Switzerland) for quantifications using numeric x3 zoom applied to the original image (Figure 1G). Only fully identifiable fibers were quantified, and diameters were randomly selected and measured through unidirectional length, without selection criteria (shortest or longest diameter). For some acquisitions, a quick fluoromyelin (20 min, 1:200, Invitrogen Carlsbad, United States), (rinsed 3×10 min in PBS) staining was added to observe eventual co-localization.

Fluoromyelin Staining

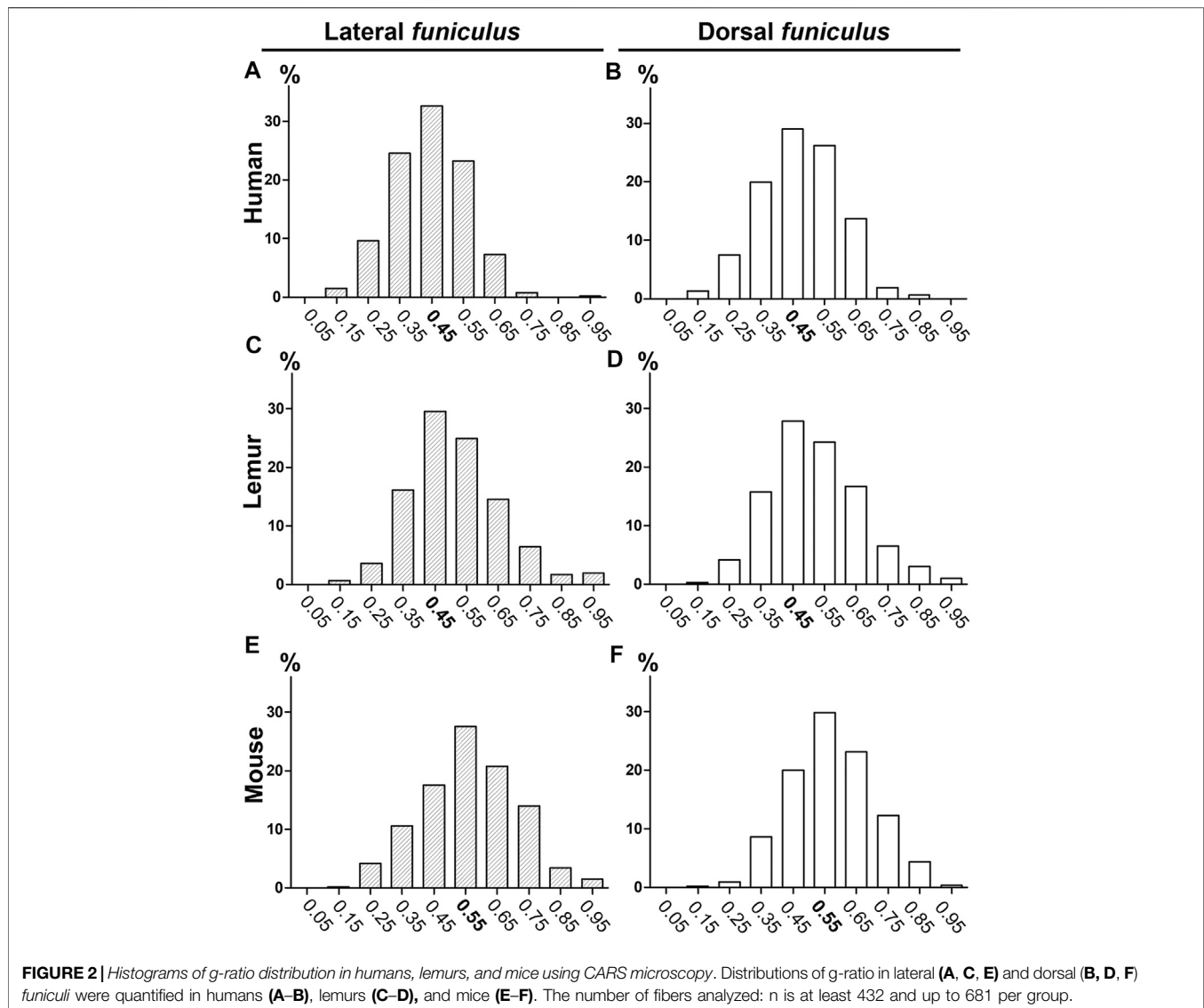
We imaged $14 \mu\text{m}$ -thick axial spinal cord cryosections of the same individuals as for CARS analysis for all species. Sections were incubated 20 min with fluoromyelin (1:200, Invitrogen, Carlsbad, United States), rinsed 3×10 min in PBS and mounted with fluorosave (Dako, Glostrup, Denmark). Images were acquired with THUNDER Imager 3D (Leica, Wetzlar, Germany; lens x 63). For all species, one field of $600 \mu\text{m} \times 400 \mu\text{m}$ was acquired in the lateral funiculus and one field of $600 \mu\text{m} \times 200 \mu\text{m}$ in the dorsal funiculus. In each field, a picture of $200 \mu\text{m} \times 200 \mu\text{m}$ located in the center of the image was taken for quantification, and 40 fibers were randomly selected and measured per location and sample. ImageJ software was used (National Institutes of Health, United States) for quantifications using numeric zoom to reach 300% of the original image. Diameter measurements were done for CARS analysis.

Three-Dimensional Illustration

3D image processing software Imaris x64 7.2.2 (Bitplane AG, Zürich, Switzerland) was used for illustration (Supplementary Figure S1).

Statistics

For CARS analysis, at least 432 fibers were quantified per anatomical location and species (3 individuals per species) [number of fibers analyzed: mice (DF = 432; LF = 481);



Microcebus murinus (DF = 643; LF = 681); human (DF = 544; LF = 580)]. Significance was accepted at $p \leq 0.05$. Results are expressed as mean \pm standard error of the mean. Student's paired (comparison within a given species) or unpaired (comparison between species) t -tests with Welch's correction were used. For fluoromyelin analysis, 120 fibers (40 for each individual) per anatomical location and species were quantified.

RESULTS

Coherent Anti-Stokes Raman Scattering Imaging Allows Discriminating Myelin Across Species Through G-Ratio Measurement

We first compared coherent anti-stokes Raman scattering (CARS) imaging (Figure 1A, fast scanning mosaic) with standard

histological methods to detect myelin, including Luxol fast blue staining (Figure 1B). The dorsal (Figures 1C–E) and lateral (Figures 1C, F) funiculi were analyzed on axial sections of the thoracic spinal cord of humans (Figures 1A, D; Supplementary Figure S1A–D), lemurs (*Microcebus murinus*) (Figure 1E), and mice (Figure 1F). We then calculated the g-ratio on numerically zoomed images (ratio of the inner-to-outer myelinated fiber diameter, Figures 1G–H) in the lateral (LF) and in dorsal (DF) funiculi in each species. No significant difference in between funiculi was observed in lemurs ($p = 0.0565$; Figure 1J) nor in mice ($p = 0.34$; Figure 1K). Conversely, in humans, the g-ratio was higher in dorsal than in lateral funiculus ($p = 0.0029$, mean g-ratio DF = 0.48 ± 0.005 ; mean g-ratio LF = 0.45 ± 0.005 ; Figure 1I), that may reflect differences in conduction speed in between funiculi. For each species, no major difference in the distribution of the g-ratio between the lateral and the dorsal funiculi was observed (Figure 2). However, g-ratio between 0.4 and 0.5 (0.45) was the most prevalent in both funiculi in humans (Figures 2A,B) and lemurs (Figures

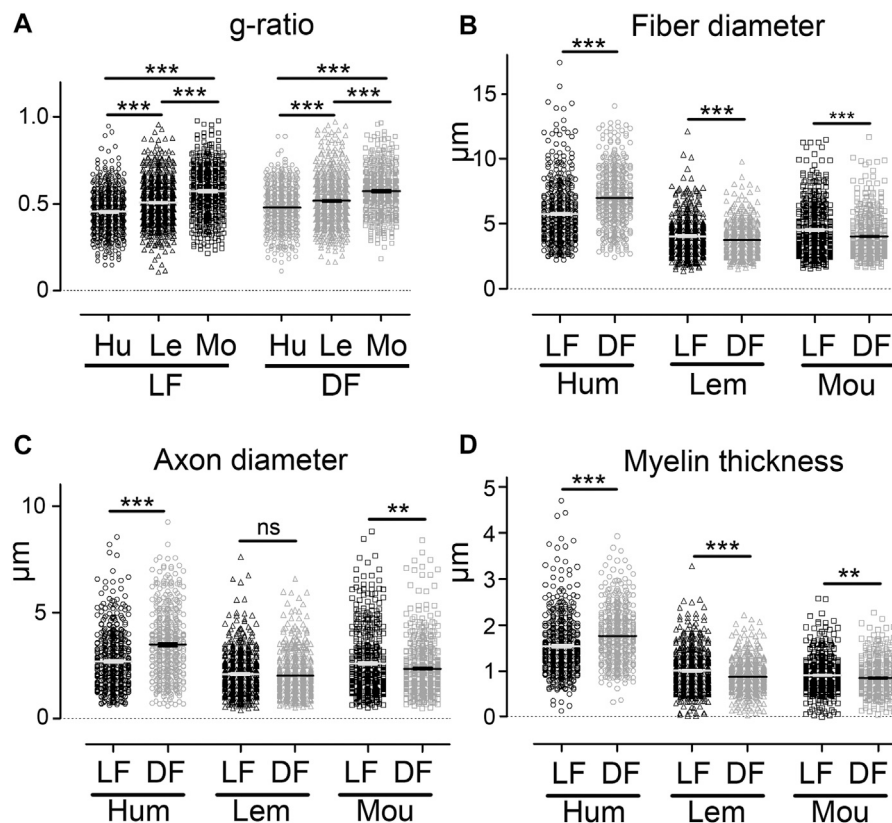


FIGURE 3 | Comparison of *g*-ratio, fiber diameter, axon diameter, and myelin thickness between species using CARS microscopy. Comparison of *g*-ratio in the lateral and dorsal *funiculi* in between humans, lemurs, and mice (A). Comparison of fiber diameter in the lateral and dorsal *funiculi* in humans, lemurs, and mice (B). Comparison of axon diameter in the lateral and dorsal *funiculi* in humans, lemurs, and mice (C). Comparison of myelin thickness in the lateral and dorsal *funiculi* in humans, lemurs, and mice (D). Hu: human, Le: lemurs, and Mo: mice. Data are mean \pm SEM per section. *** $p < 0.001$, ** $p < 0.01$ ns: non-significant; unpaired *t*-test with Welch's correction. Number of fibers analyzed: *n* is at least 432 and up to 681 per group.

2C,D) contrariwise to mice (Figures 2E,F) where the peak was observed for *g*-ratio between 0.5 and 0.6 (0.55).

Spectra of G-Ratio, Fiber Diameter, Axon Diameter, and Myelin Thickness in the Three Species

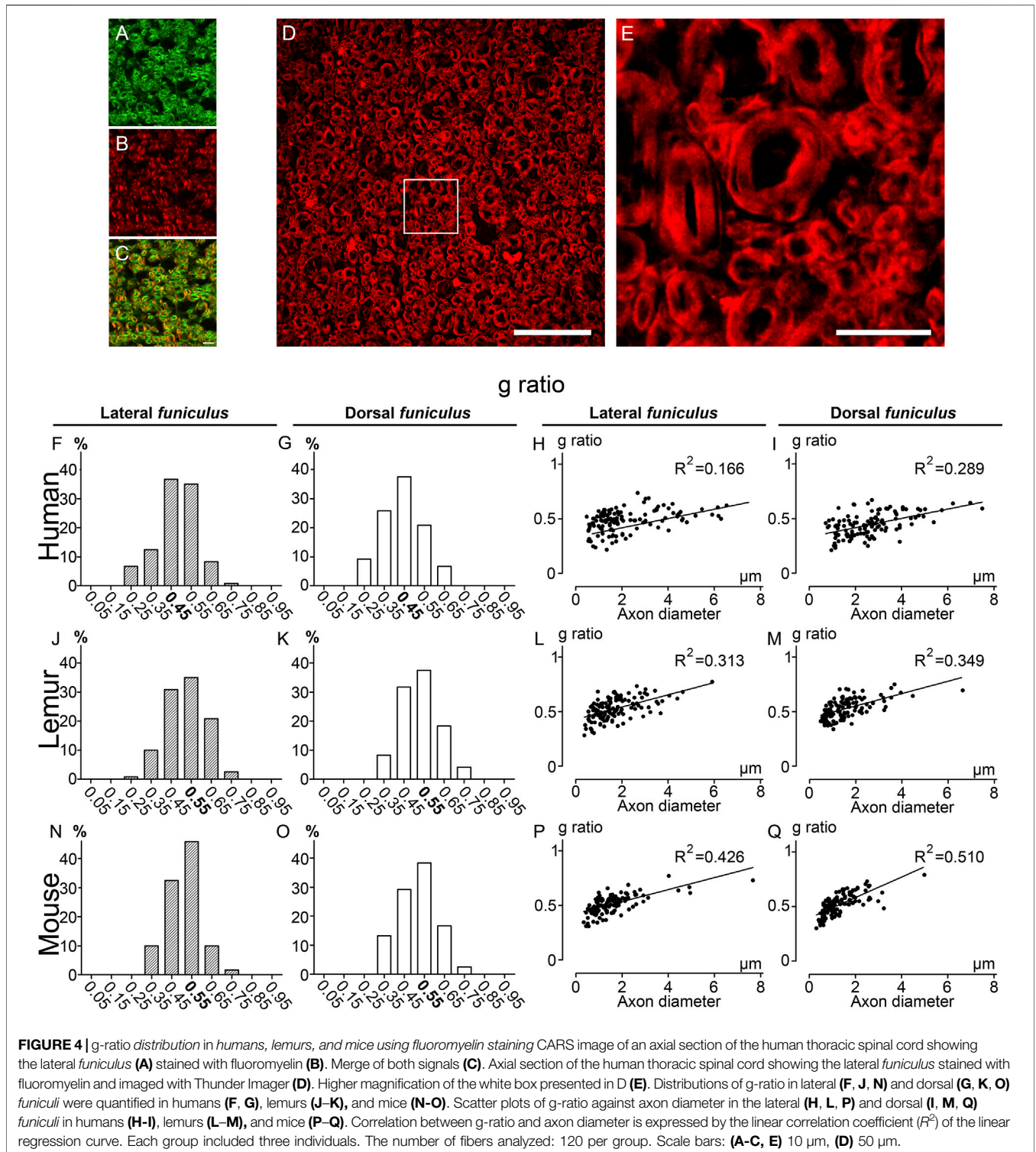
Comparison of *g*-ratio, fibers, and axons diameters (Figure 1J) in the lateral and dorsal *funiculi* (Figure 3) also highlighted species specificities. In both *funiculi*, *g*-ratio was lower in humans than in lemurs than in mice (Figure 3A, $p < 0.001$ for all comparisons); that may reflect differences in conduction speed in between species. Moreover, in humans, fiber and axon diameters, as well as myelin thickness, were higher in the dorsal (fiber diameter: $6.99 \pm 0.09 \mu\text{m}$, axon diameter: $3.47 \pm 0.07 \mu\text{m}$ and myelin thickness: $1.77 \pm 0.03 \mu\text{m}$) as compared to the lateral *funiculus* (fiber diameter: $5.78 \pm 0.10 \mu\text{m}$, axon diameter: $2.69 \pm 0.06 \mu\text{m}$ and myelin thickness: $1.54 \pm 0.03 \mu\text{m}$) (Figures 3B-D, $p < 0.001$ for all parameters). In mice, all parameters were lower in the dorsal *funiculus* (fiber diameter: $4.03 \pm 0.07 \mu\text{m}$, axon diameter: $2.35 \pm 0.06 \mu\text{m}$ and myelin thickness: $0.85 \pm 0.02 \mu\text{m}$) as compared to the lateral *funiculus* (fiber diameter: $4.52 \pm 0.09 \mu\text{m}$, axon diameter: $2.59 \pm 0.07 \mu\text{m}$ and myelin thickness: $0.91 \pm 0.018 \mu\text{m}$) (Figures

3B-D, $p < 0.001$ for all parameters). In lemurs, fiber diameter (DF: $3.75 \pm 0.05 \mu\text{m}$ and LF: $4.04 \pm 0.06 \mu\text{m}$) and myelin thickness (DF: $0.87 \pm 0.014 \mu\text{m}$ and LF: $1.00 \pm 0.02 \mu\text{m}$) were lower in the dorsal as compared to the lateral *funiculus*; no difference was detectable in axon diameter between *funiculi* (DF: $2.01 \pm 0.04 \mu\text{m}$ and LF: $2.09 \pm 0.04 \mu\text{m}$) (Figures 3B-D).

Taken together, these data demonstrate that using CARS to compare fiber and axon diameters as well as myelin thickness allows interspecies discrimination of three healthy mammal spinal cords.

Fluoromyelin Analysis Display Similar G-Ratio Values as Coherent Anti-Stokes Raman Scattering Imaging

To confirm the accuracy of CARS imaging, we then carried out in the same samples, *g*-ratio analysis using fluoromyelin staining; another method that, similar to CARS, does not require resin embedding and dehydration and permits to visualize myelin (Figure 4). In the first step, we acquired simultaneously CARS (Figure 4A) and fluoromyelin staining (Figure 4B), both signals partly co-localized (Figure 4C). We then used a Thunder imager with computational clearing to obtain images without out-of-focus



blur (Figures 4D,E; Supplementary Figures 1E-H) and to measure g-ratio in the same samples used for CARS analysis. We confirmed for each species the absence of difference in g-ratio distribution between both funiculi (Figures 4F, G, humans; J&K; lemurs and N&O; mice). Moreover, similarly to CARS quantifications, a g-ratio in between 0.4 and 0.5 (0.45) was the most prevalent in both funiculi

in humans (Figures 4F, G); for lemurs, the g-ratio in both funiculi was predominantly at 0.55 (however, the proportion of fibers presenting a g-ratio of 0.45 was almost identical) (Figures 4J, K); finally, in mice, the peak was observed for g-ratio at 0.55 (Figures 4). Linear regression curves of g-ratio against axon's diameter highlighted that lemurs display characteristics (Figures 4L-M; LF

$R^2 = 0.313$ and $DF R^2 = 0.349$) in between human (Figures 4H–I; LF $R^2 = 0.166$ and $DF R^2 = 0.289$) and mice (Figures 4P–Q; LF $R^2 = 0.426$ and $DF R^2 = 0.510$). Taken together, these data demonstrate that CARS is a label-free alternative to other microscopy techniques that allow to discrimination of myelinated fibers across species in the mammal spinal cord *funiculi*.

DISCUSSION

Here, we present the first CARS analysis of spinal cord myelin in two white matter tracts (lateral and dorsal *funiculi*) of three different species, i.e., mice, lemurs, and humans. We identified species specificities in particular regarding values of the g-ratio and thus confirmed the accuracy of CARS imaging as an alternative to other microscopy techniques to assess and compare myelin across species.

G-Ratio Coincides with Species Evolution and Myelin Fibers Differ within the Same Species According to Their Location

Myelin fibers g-ratio of both *funiculi* was higher in mice than in lemurs than in humans and thus inversely coincides with species evolution. This may partly reflect differences in fiber conduction speed across species. Indeed, a few studies have demonstrated that the g-ratio is not only a key determinant for the conduction velocity of a fiber [3,35,36] but also optimized for speed of signal conduction, cellular energetics, and spatial constraints [37]. The distribution of the g-ratio within lateral or dorsal *funiculi* in the three species highlighted a similar repartition in humans and in lemurs by opposition to mice. Moreover, we identified a higher g-ratio in dorsal as compared to the lateral *funiculus* only in humans. Conversely, no difference in g-ratio is observed between the lateral and the dorsal *funiculus* in mice and lemurs. Fibers and axons diameters, as well as myelin thickness, are higher in the dorsal *funiculus* in humans. This observation certainly mirrors anatomical differences in fiber tracts displaying sensory motor functions and may reflect species-specificities of conduction velocity of myelin fibers.

Taken together, structural similarities between humans and lemurs central nervous system confirms the necessity to develop non-human primate models to study CNS diseases such as demyelinating disease, traumatic brain injury, and spinal cord injury. This is particularly important when studying spinal cord disorders since closer anatomical and functional characteristics of the motor systems, including the corticospinal tract, is observed between human and non-human primate as opposed to rodent [38].

Coherent Anti-Stokes Raman Scattering Microscopy, an Alternative Method to Analyze Myelin

A neuroimaging method, termed multi-component-driven equilibrium single-pulse observation of T1 and T2 (mcDESPOT), allows to examine myelin water fraction (MWF) as an *in vivo* metric of myelin integrity and content [39,40]. It has been demonstrated that a combination of magnetic

resonance (MR) markers that are sensitive to the myelin volume fraction (MVF) and to the intra-axonal volume fraction (AVF) is sufficient to compute a g-ratio for each voxel (aggregate g-ratio). However, it does not allow estimating axon diameter, myelin sheath thickness, and pitfalls of g-ratio imaging such as MR artifacts, lack of specificity, low spatial resolution, and long acquisition times remain [37]. Thus, as suggested recently [18], the emergence of exhaustive databases of myelin fibers structure using several modalities of investigation tools will facilitate further validation of non-invasive methods such as magnetic resonance imaging.

The overall lower g-ratio values (about 0.5) that we obtained using both CARS and fluoromyelin staining as compared to those obtained using electron microscopy may result from variation in factors such as fixative, embedding, and dehydration steps. As recently reviewed, methods that do not require staining, embedding, and dehydration, which are all critical steps for myelin damage, may provide accurate measurement of parameters such as g-ratio and myelin sheath thickness [for review see [18]]. Slight differences in g-ratio repartition that we observed when using CARS imaging and fluoromyelin; in particular with lemurs, may thus also reflect differences in tissue processing. Indeed, even if both techniques do not require resins embedding and dehydration, conversely to CARS, fluoromyelin is not a label-free method and requires mounting.

In conclusion, this study compared the first-time spinal cord myelin sheath in three different species using a label-free method and thus represents a new biological application of a label-free method in the field of spinal cord analysis. We identified species differences between axon and fiber diameters, myelin thickness, and g-ratio that may reflect species-specificities of conduction velocity of myelin fibers. The combination of several imaging techniques, including CARS, will thus permit to better characterize myelin structure in healthy conditions and its alterations in diseases.

DATA AVAILABILITY STATEMENT

The raw data supporting the conclusion of this article will be made available by the authors without undue reservation.

ETHICS STATEMENT

The studies involving human samples collection were reviewed and approved by the “Agence de la Biomédecine” (PFS-ssNUM-BAUCHET). Written informed consent for participation was not required for this study in accordance with the national legislation and the institutional requirements. The animal study was reviewed and approved by the Veterinary Services Department of Hérault, the regional ethic committee n°36 for animal experimentation, and the French Ministry of National Education, Higher Education and Research (authorizations; mice: n°34118 and non-human primates n° APAFIS#16177-2018071810113615v3). Experiments followed the European legislative, administrative, and statutory measures for animal experimentation (EU/Directive/2010/63) and the ARRIVE guidelines.

AUTHOR CONTRIBUTIONS

GP participated in the design of the project and in human samples collection, analyzed the data, and contributed to the writing of the manuscript; YG contributed to the design of the project as well as acquisition and analysis of the data; J-CP participated in the acquisition and analysis of the data; KO participated in the quantification of the data; NL participated in human samples collection; FV-L coordinated human samples collection; HB designed CARS acquisition and participated in the analysis, and FP conceptualized the research, designed the project, participated in the analysis and data interpretation, drafting the work and final approval.

FUNDING

This work was supported by the patient organizations “Demain Debout Aquitaine” (to YG and FP) and “Verticale” (to YG and

FP). The funding sources were not involved in study design, collection, analysis, and interpretation of data and the writing of the report and in the decision to submit the article for publication.

ACKNOWLEDGMENTS

We thank the “Agence de la Biomédecine” for organization of human samples collection. We thank Fabrice Bardin and the “Montpellier Ressources Imagerie” for advices in CARS acquisition. We also thank Nadine Mestre-Frances for her expertise in non-human primates.

SUPPLEMENTARY MATERIAL

The Supplementary Material for this article can be found online at: <https://www.frontiersin.org/articles/10.3389/fphy.2021.665650/full#supplementary-material>

REFERENCES

- O'Brien JS, and Sampson EL. Lipid composition of the normal human brain: gray matter, white matter, and myelin. *J Lipid Res* (1965) 6:537–44. doi:10.1016/s0022-2275(20)39619-x
- Harayama T, and Riezman H. Understanding the diversity of membrane lipid composition. *Nat Rev Mol Cel Biol* (2018) 19:281–96. doi:10.1038/nrm.2017.138
- Rushton WAH. A theory of the effects of fibre size in medullated nerve. *J Physiol* (1951) 115:101–22. doi:10.1113/jphysiol.1951.sp004655
- Marangon D, Boccazzi M, Lecca D, and Fumagalli M. Regulation of Oligodendrocyte Functions: Targeting Lipid Metabolism and Extracellular Matrix for Myelin Repair. *J Clin Med* (2020) 9(2):470. doi:10.3390/jcm9020470
- Saab AS, and Nave K-A. Myelin dynamics: protecting and shaping neuronal functions. *Curr Opin Neurobiol* (2017) 47:104–12. doi:10.1016/j.conb.2017.09.013
- Morrison BM, Lee Y, and Rothstein JD. Oligodendroglia: metabolic supporters of axons. *Trends Cel Biol* (2013) 23:644–51. doi:10.1016/j.tcb.2013.07.007
- Micu I, Plemel JR, Caprariello AV, Nave KA, and Stys PK. Axo-myelinic neurotransmission: a novel mode of cell signalling in the central nervous system. *Nat Rev Neurosci* (2017) 19:58. doi:10.1038/nrn.2017.128
- Stimmer L, Fovet C-M, and Serguera C. Experimental Models of Autoimmune Demyelinating Diseases in Nonhuman Primates. *Vet Pathol* (2018) 55:27–41. doi:10.1177/0300985817712794
- Klüver H, and Barrera E. A method for the combined staining of cells and fibers in the nervous system. *J Neuropathol Exp Neurol* (1953) 12:400–3. doi:10.1097/00005072-195312040-00008
- Meier C. Some observations on early myelination in the human spinal cord. Light and electron microscope study. *Brain Res* (1976) 104:21–32. doi:10.1016/0006-8993(76)90644-2
- Hori SH. A Simplified Acid Hematein Test for Phospholipids. *Stain Tech* (1963) 38:221–5. doi:10.3109/10520296309061182
- Gallyas F. Silver staining of myelin by means of physical development. *Neurol Res* (1979) 1:203–9. doi:10.1080/01616412.1979.11739553
- Thetiot M, Freeman SA, and Desmazières A. Immunohistochemical Analysis of Myelin Structures. *Methods Mol Biol* (2018) 1791:15–23. doi:10.1007/978-1-4939-7862-5_2
- Fluri F, Ferracin F, Erne B, and Steck AJ. Microheterogeneity of anti-myelin-associated glycoprotein antibodies. *J Neurol Sci* (2003) 207:43–9. doi:10.1016/s0022-510x(02)00359-3
- Zumbusch A, Holtom GR, and Xie XS. Three-Dimensional Vibrational Imaging by Coherent Anti-Stokes Raman Scattering. *Phys Rev Lett* (1999) 82:4142–5. doi:10.1103/physrevlett.82.4142
- Evans CL, and Xie XS. Coherent anti-stokes Raman scattering microscopy: chemical imaging for biology and medicine. *Annu Rev. Anal. Chem.* (2008) 1: 883–909. doi:10.1146/annurev.anchem.1.031207.112754
- Bégin S, Bélanger E, Laffray S, Vallée R, and Côté D. In vivo optical monitoring of tissue pathologies and diseases with vibrational contrast. *J Biophoton* (2009) 2:632–42. doi:10.1002/jbio.200910071
- Saliani A, Perraud B, Duval T, Stikov N, Rossignol S, and Cohen-Adad J. Axon and Myelin Morphology in Animal and Human Spinal Cord. *Front Neuroanat* (2017) 11:129. doi:10.3389/fnana.2017.00129
- Brideau C, Poon KWC, Colarusso P, and Stys PK. Excitation parameters optimized for coherent anti-Stokes Raman scattering imaging of myelinated tissue. *J Biomed Opt* (2019) 24:1–8. doi:10.1117/1.jbo.24.4.046502
- Bégin S, Dupont-Therrien O, Bélanger E, Daradich A, Laffray S, De Koninck Y, et al. Automated method for the segmentation and morphometry of nerve fibers in large-scale CARS images of spinal cord tissue. *Biomed Opt Express* (2014) 5:4145–61. doi:10.1364/boe.5.004145
- Wang H, Fu Y, Zickmund P, Shi R, and Cheng J-X. Coherent anti-stokes Raman scattering imaging of axonal myelin in live spinal tissues. *Biophysical J* (2005) 89:581–91. doi:10.1529/biophysj.105.061911
- Fu Y, Huff TB, Wang H-W, Cheng J-X, and Wang H. *Ex vivo* and *in vivo* imaging of myelin fibers in mouse brain by coherent anti-Stokes Raman scattering microscopy. *Opt Express* (2008) 16:19396–409. doi:10.1364/oe.16.019396
- Shi Y, Zhang D, Huff TB, Wang X, Shi R, Xu X-M, et al. Longitudinal *in vivo* coherent anti-Stokes Raman scattering imaging of demyelination and remyelination in injured spinal cord. *J Biomed Opt* (2011) 16:106012. doi:10.1117/1.3641988
- Picardi G, Spalloni A, Generosi A, Paci B, Mercuri NB, Luce M, et al. Tissue degeneration in ALS affected spinal cord evaluated by Raman spectroscopy. *Sci Rep* (2018) 8:13110. doi:10.1038/s41598-018-31469-4
- Fu Y, Frederick TJ, Huff TB, Goings GE, Miller SD, and Cheng J-X. Paranodal myelin retraction in relapsing experimental autoimmune encephalomyelitis visualized by coherent anti-Stokes Raman scattering microscopy. *J Biomed Opt* (2011) 16:106006. doi:10.1117/1.3638180
- Poon KWC, Brideau C, Klaver R, Schenk GJ, Geurts JJ, and Stys PK. Lipid biochemical changes detected in normal appearing white matter of chronic multiple sclerosis by spectral coherent Raman imaging. *Chem Sci* (2018) 9: 1586–95. doi:10.1039/c7sc03992a
- Perrin FE, Gerber YN, Teigell M, Lonjon N, Boniface G, Bauchet L, et al. Anatomical study of serotonergic innervation and 5-HT1A receptor in the

- human spinal cord. *Cell Death Dis* (2011) 2:e218, 2011 . e218. doi:10.1038/cddis.2011.98
28. Gerber YN, Saint-Martin GP, Bringuier CM, Bartolami S, Goze-Bac C, Noristani HN, et al. CSF1R Inhibition Reduces Microglia Proliferation, Promotes Tissue Preservation and Improves Motor Recovery after Spinal Cord Injury. *Front Cel Neurosci* (2018) 12:368. doi:10.3389/fncel.2018.00368
 29. Noristani HN, Saint-Martin GP, Cardoso M, Sidiboulenouar R, Cateau M, Coillot C, et al. Longitudinal MRI analysis and histological characterization after spinal cord injury in two mouse strains with different functional recovery: gliosis as a key factor. *J Neurotrauma* (2018).
 30. Mytskaniuk V, Bardin F, Boukhaddaoui H, Rigneault H, and Tricaud N. Implementation of a Coherent Anti-Stokes Raman Scattering (CARS) System on a Ti:Sapphire and OPO Laser Based Standard Laser Scanning Microscope. *J Vis Exp* (2016). doi:10.3791/54262
 31. Dudovich N, Oron D, and Silberberg Y. Single-pulse coherently controlled nonlinear Raman spectroscopy and microscopy. *Nature* (2002) 418:512–4. doi:10.1038/nature00933
 32. Lim S-H, Caster AG, Nicolet O, and Leone SR. Chemical imaging by single pulse interferometric coherent anti-stokes Raman scattering microscopy. *J Phys Chem B* (2006) 110:5196–204. doi:10.1021/jp057493k
 33. Volkmer A, Cheng J-X, and Xie XS. Vibrational Imaging with High Sensitivity via Epidetected Coherent Anti-Stokes Raman Scattering Microscopy. *Phys Rev Lett* (2001) 87. doi:10.1103/physrevlett.87.023901
 34. Cheng J-X, and Xie XS. *Coherent Anti-stokes Raman Scattering Microscopy: Instrumentation, Theory, and Applications*, 108 (2004). doi:10.1021/jp035693v
 35. Goldman L, and Albus JS. Computation of impulse conduction in myelinated fibers; theoretical basis of the velocity-diameter relation. *Biophysical J* (1968) 8: 596–607. doi:10.1016/s0006-3495(68)86510-5
 36. Chomiak T, and Hu B. What is the optimal value of the g-ratio for myelinated fibers in the rat CNS? A theoretical approach. *PLoS One* (2009) 4:e7754. doi:10.1371/journal.pone.0007754
 37. Campbell JSW, Leppert IR, Narayanan S, Boudreau M, Duval T, Cohen-Adad J, et al. Promise and pitfalls of g-ratio estimation with MRI. *Neuroimage* (2018) 182:80–96. doi:10.1016/j.neuroimage.2017.08.038
 38. Friedli L, Rosenzweig ES, Barraud Q, Schubert M, Dominici N, Awai L, et al. Pronounced species divergence in corticospinal tract reorganization and functional recovery after lateralized spinal cord injury favors primates. *Sci Transl Med* (2015) 7:302ra134, 2015. 302ra134. doi:10.1126/scitranslmed.aac5811
 39. Deoni SCL, Rutt BK, Arun T, Pierpaoli C, and Jones DK. Gleaning multicomponent T 1 and T 2 information from steady-state imaging data. *Magn Reson Med* (2008) 60:1372–87. doi:10.1002/mrm.21704
 40. Denic A, Macura SI, Mishra P, Gamez JD, Rodriguez M, and Pirko I. MRI in rodent models of brain disorders. *Neurotherapeutics* (2011) 8:3–18. doi:10.1007/s13311-010-0002-4
- Conflict of Interest:** The authors declare that the research was conducted in the absence of any commercial or financial relationships that could be construed as a potential conflict of interest.
- Publisher's Note:** All claims expressed in this article are solely those of the authors and do not necessarily represent those of their affiliated organizations, or those of the publisher, the editors and the reviewers. Any product that may be evaluated in this article, or claim that may be made by its manufacturer, is not guaranteed or endorsed by the publisher.
- Copyright © 2021 Poulen, Gerber, Perez, Oubarrahou, Lonjon, Vachery-Lahaye, Boukhaddaoui and Perrin. This is an open-access article distributed under the terms of the Creative Commons Attribution License (CC BY). The use, distribution or reproduction in other forums is permitted, provided the original author(s) and the copyright owner(s) are credited and that the original publication in this journal is cited, in accordance with accepted academic practice. No use, distribution or reproduction is permitted which does not comply with these terms.